Ultrasonic wave transport in a system of disordered resonant scatterers: Propagating resonant modes and hybridization gaps

M. L. Cowan,[1,*] J. H. Page,[1,†] and Ping Sheng[2]
[1]*Department of Physics and Astronomy, University of Manitoba, Winnipeg, Manitoba R3T 2N2, Canada*
[2]*Department of Physics, Hong Kong University of Science and Technology, Clear Water Bay, Kowloon, China*
(Received 1 March 2011; published 19 September 2011)

We present the results of ultrasonic pulse propagation experiments on suspensions of plastic spherical scatterers immersed in water. This system was selected to study the effects of scattering resonances on wave transport. By separating the coherent ballistic component from the multiply scattered wave field, both the dispersion relations and the diffusive propagation of ultrasound were investigated. We show that the dispersion relation is marked by a series of hybridization gaps due to the coupling between the propagating modes of surrounding fluid and the scattering resonances. Effects of dissipation on the formation of the gaps were investigated. We find evidence in our ultrasonic data for the existence of a (slowly propagating) second longitudinal mode, also seen in Brillouin scattering experiments, that arises from the coupling between the resonant scatterers. These results are interpreted with an effective medium model based on the spectral function approach, which gives an excellent description of the dispersion relations in this system. Measurements of the multiply scattered ultrasound allow both the diffusion coefficient and the absorption time to be measured as a function of frequency. The relationship between the diffusion coefficient and the ballistic data is discussed, while the measurement of the absorption time from the decay of the multiply scattered coda enables the absorption and scattering lengths to be separated. These ultrasonic measurements and their interpretation based on the spectral function approach give a very complete picture of wave transport in this strongly scattering resonant system.

DOI: 10.1103/PhysRevB.84.094305 PACS number(s): 43.35.+d, 43.20.+g, 63.50.−x, 82.70.Kj

I. INTRODUCTION

The last two decades have seen remarkable progress in the study of classical wave transport through strongly scattering media, both random and ordered.[1,2] One of the important problems continues to be the role of scattering resonances on the transport of waves through the medium. The coupling between scattering resonances and propagating waves in the medium surrounding the scatterers can lead to the formation of band gaps, often referred to as hybridization gaps. The underlying mechanism can be viewed as level repulsion when two bands of the same symmetry cross each other. Such hybridization gaps have recently attracted growing interest in the context of phononic crystals,[3–6] where they provide an alternate mechanism to Bragg scattering for the formation of band gaps. Scattering resonances are also central to the properties of metamaterials,[7] where the resonances occur at low frequencies such that the wavelength is much larger than the size of the scatterers—this facilitates an effective medium description of the transport and can lead to remarkable properties, such as a negative index of refraction[8] and a highly efficient blocking of low-frequency sound.[9,10]

Compared with ordered materials, random systems have an advantage for studying hybridization gaps and related phenomena, since their observation is not potentially confounded by Bragg scattering. For fundamental studies, ultrasonic techniques also have some advantages since they can readily detect the wave field (not just the intensity), perform experiments resolved in both time and space, and study systems on a convenient range of length scales that facilitate the control of the properties of the scattering medium over a wide range of scattering contrasts. One example is suspensions of plastic spheres randomly dispersed in a liquid, which show rich acoustic behavior in the strongly scattering intermediate frequency regime.[11–15] The origin of this interesting behavior lies in the strong acoustic scattering resonances of plastic spheres in a liquid. Previous Brillouin scattering measurements of the acoustic dispersion curves in these systems have revealed that at certain wavelengths there can be two propagating modes.[11,14] These modes have been identified as a fast longitudinal mode with phase velocity in between the velocities of the plastic and liquid components and a slower Stoneley or interfacial wave mode, which arises from the coupling of the neighboring plastic sphere resonances.[12,13] It has also been found that a very pronounced gap appears in the fast mode, coinciding with the appearance of the coupled Stoneley mode. Even though these phenomena occur at intermediate frequencies in this system, where the wavelength is comparable with the size of the scatterers, the experimental results have been successfully modeled by an effective medium model based on a spectral function approach, which enables the dispersion curve to be calculated by finding the peaks in the spectral function of the system.[12,13,16,17]

Figure 1 shows the calculated spectral function for polymethylmethacrylate (PMMA) spheres randomly packed in water. The peaks of the spectral function delineate the dispersion curves of the propagating modes (or more precisely quasimodes since the modes have a finite width due to scattering) because, for these values of ω and k, the peaks correspond to modes with the least scattering. Since the widths and heights of the peaks vary with frequency, and the direction of the change in peak height is parallel to neither the frequency nor the wave vector axes, different types of experiments may measure different dispersion relations.[17] Two cases are illustrated in Fig. 1, where the dashed line shows the results of finding the peak frequencies by scanning the spectral function at constant k, while the solid line shows the results of constant frequency scans. Brillouin scattering measures

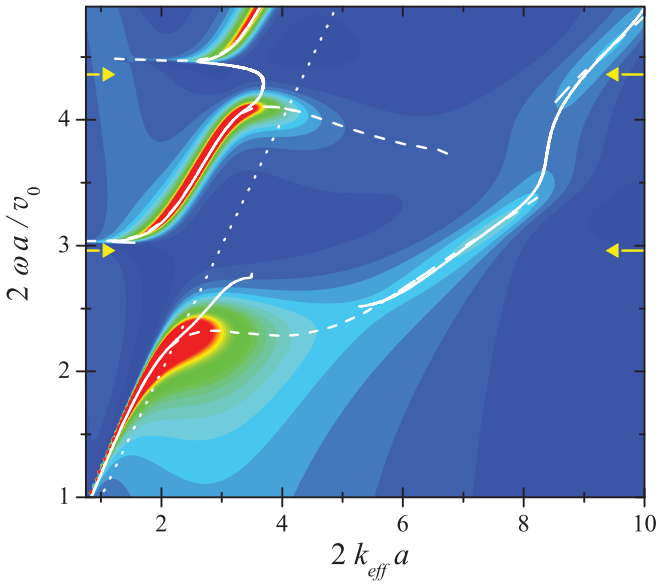

FIG. 1. (Color online) Spectral function calculated without absorption for a system consisting of PMMA spheres randomly packed in water at a volume fraction of 0.55. The solid line shows the peaks in the spectral function found by holding ω constant and scanning through k. The dashed line shows the peaks found when holding k constant. The dotted line gives the dispersion relation for water, and the horizontal arrows indicate the resonant frequencies of a single PMMA sphere in water.

the modal frequency at a constant wave vector selected by the scattering angle between the incident and scattered light beams, and so it measures the dashed dispersion curve. By contrast, ultrasonic transmission measurements are performed by inputting a wave at a particular frequency (or band of frequencies in the case of a pulsed experiment) and measuring the corresponding phase shift of the transmitted wave, from which the wave vector is determined. Therefore, ultrasonic experiments measure the solid dispersion curve shown in Fig. 1 and can reveal complementary information on the dispersion relations and transport properties to that obtained by Brillouin scattering experiments. The two dispersion curves can be quite different at frequencies near the band gaps and especially in the region where the Stoneley mode first appears, but both methods of determining the dispersion relations predict a gap in the fast longitudinal mode centered at $2\omega a/v_0 = 2.8$. Here, ω is the angular frequency, a is the radius of the solid spheres, and v_0 is the speed of sound in the liquid.

We denote this gap the hybridization gap, arising from the interaction between the propagating mode in the water-sphere mixture and the (Stoneley) resonance of the spheres. In the present case, the resonances on neighboring spheres couple and form another propagating mode with its own dispersion relation. The simple picture of level repulsion would give rise to the gap. It will be seen later, however, that when there is absorption in the system, a propagating mode can appear in the gap, i.e. the gap closes. This apparently paradoxical result can be explained by noting that, since absorption can be modeled by an imaginary part of the modulus, the evanescent wave vector (for the evanescent mode in the gap) acquires an imaginary part, i.e. a propagating component. Such a propagating mode in the hybridization gap is precisely what has been measured in our experiments; it is also predicted in the spectral function model by using a complex modulus to describe the constituent materials with the imaginary component given by measured absorption constant.

This paper describes the results of ultrasonic pulse transmission experiments to investigate these phenomena by measuring wave transport in a strongly scattering dispersion of plastic spheres. By using ultrasonic pulses, we are able to efficiently separate the coherent ballistic pulse from the multiply scattered sound.[17,18] This allows us to measure the dispersion curves in the strongly scattering regime and therefore explore the band gaps in the fast mode that arise from the hybridization of the resonances and the water dispersion curve as well as from the properties of the unusual slow mode. Even though the multiply scattered component of the total transmitted wave field is surprisingly small, we are able to determine the time-dependent intensity profile and model it using the diffusion approximation, enabling the average diffusion coefficient and absorption time to be measured. Thus, our experiments and modeling using the spectral function approach give a remarkably complete picture of the effects of hybridization on wave transport in this strongly scattering resonant system.

In what follows, sample preparation and measurements of the ballistic and multiply scattered components of the transmitted waves are described in Sec. II. In Sec. III, we show that the ballistic component of the waves can be successfully modeled by the spectral function approach with scattering loss being the main source of extinction. The multiply scattered component, on the other hand, is very well described within the framework of diffusive behavior. Relevant underlying physics is discussed. We conclude in Sec. IV by summarizing the main points of our work.

II. EXPERIMENTS

A. Ballistic measurements

Samples were prepared using two different kinds of plastic beads. The first set of samples was made using PMMA spheres, which were sieved from a polydisperse distribution of spheres to limit the diameter to the range 0.180 to 0.212 mm, giving a mean diameter $2a = 0.196$ mm. The spheres were randomly packed in water at a volume fraction of 0.55 between two thin plastic walls, which were separated by a spacer that controlled the sample thickness. We prepared two samples with thicknesses of 2.46 and 0.56 mm. The longitudinal velocity in bulk PMMA is 2.75 mm/μs, the transverse velocity is 1.1 mm/μs, and the density is 1.19 g/ml. Our second set of samples was prepared using very monodisperse 1.2-mm-diameter acetate beads. Acetate has similar transport properties with a longitudinal velocity of 2.50 mm/μs, a shear velocity of 1.05 mm/μs, and a density equal to 1.28 g/ml. These two kinds of plastic thus have almost the same ultrasonic scattering properties, and the samples made with them exhibit the same qualitative and very similar quantitative behaviors. There is a strong acoustic impedance (ρv) mismatch between the spheres and the water, which has a sound velocity, $v_0 = 1.49$ mm/μs, and a density of 1.0 g/ml. In particular, the shear velocity in the solid spheres is quite low and is smaller than the longitudinal

velocity of the surrounding water. Thus, we expect strong scattering resonances when the wavelength λ is comparable to the sphere size.

The experiments were performed with the samples immersed in a tank filled with water, which provided a convenient low-loss wave transport medium between the samples and the ultrasonic planar transducers. The samples were placed in the far field of the transducers. One of the transducers generated the ultrasonic pulses, which had a broad quasiplanar profile when they reached the samples, and the other transducer detected the transmitted ultrasound. The sound transmitted through the sample is a superposition of the coherent ballistic component plus the multiply scattered component. When the wavelength of the sound is comparable with the sphere size, the scattering can be strong, and in order to measure the ballistic transport properties, we must separate the coherent ballistic signal from the multiply scattered waves, which follow random scattering paths through the sample.[18] Since a piezoelectric transducer measures the average wave field across its face, the spatial incoherence of the speckle pattern created by the scattered ultrasound causes it to cancel when a transducer with sufficiently large surface area is used (1-in-diameter, in our experiments), so that the remaining detected signal is the coherent ballistic wave. In cases where this spatial averaging in the detector does not completely remove the scattered signal, the field can also be ensemble averaged over different realizations of the sample; however, this was not necessary here.

Ballistic measurements were taken predominately on the PMMA samples and at frequencies spanning the range from well below to well above the position of the first gap in the fast mode. At frequencies below the gap, only one mode is observed (Fig. 2). The phase velocity at these frequencies was found by measuring the phase change of the sound transmitted

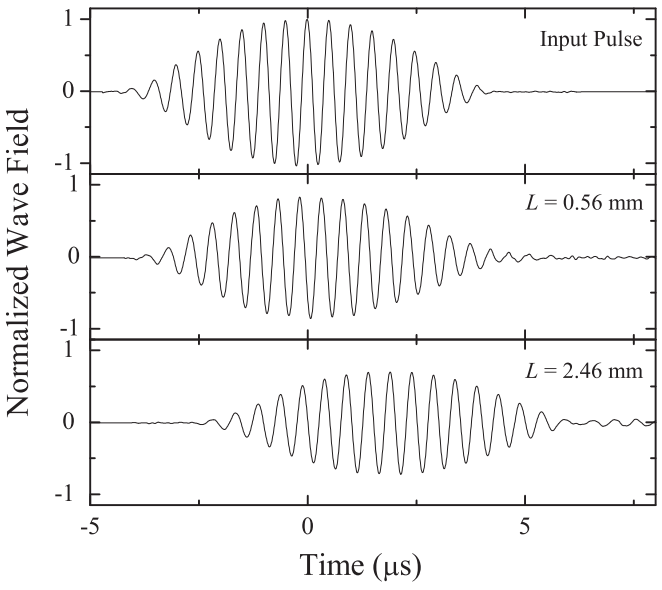

FIG. 2. Input and transmitted ballistic pulses below the gap for sample thicknesses of 0.56 mm (middle panel) and 2.46 mm (bottom panel) at a frequency of 2.0 MHz (corresponding to $2\omega a/v_0 = 1.69$). The pulse amplitudes are normalized so that the peak of the input pulse is equal to 1.

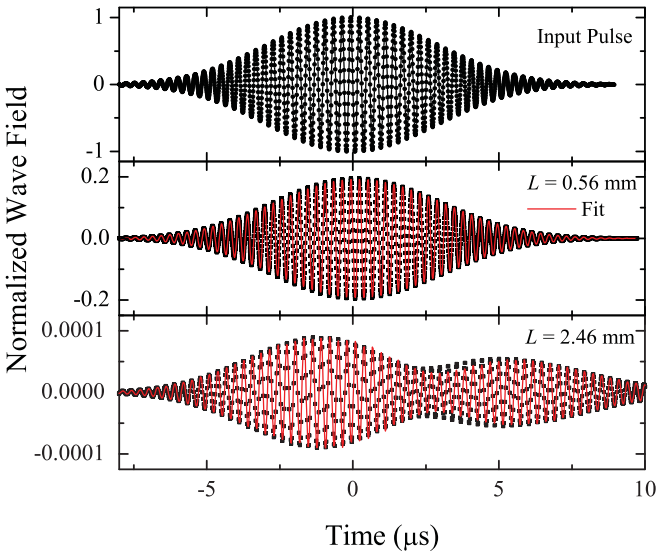

FIG. 3. (Color online) Input and transmitted ballistic pulses in the gap for sample thicknesses of 0.56 mm (middle panel) and 2.46 mm (bottom panel) at a frequency of 3.4 MHz (corresponding to $2\omega a/v_0 = 2.81$). The thicker sample shows direct evidence of two propagating modes. The pulse amplitudes are normalized so that the peak of the input pulse is equal to 1.

through each sample. The scattering mean free path l_s and group velocity v_g were also determined, using the methods described in Ref. 17. When the frequency was raised to a value in the expected gap, we detected two distinct and comparably strong ballistic modes. This is most evident from the thick sample data, as the modes have had a chance to separate in time due to their different group and phase velocities (Fig. 3). To be absolutely certain that this effect was not just due to the polydispersity of the PMMA spheres, we also performed experiments using the monodisperse acetate beads. We found similar behavior with two modes in the gap. For the mode in the hybridization gap frequency region, we shall see in Sec. III that it can be accounted for by the presence of absorption.

To interpret the two-mode data, we fit the thick sample data with two interfering, scaled versions of the input pulse, each with different velocities, amplitudes, and slightly larger widths. We used a digital filtering technique to control the bandwidth of the pulses so that the bandwidth was narrow enough to limit dispersive spreading of the pulses while keeping the width (in time) of the pulses sufficiently short that the two modes could be resolved in time for this sample. Then to check the robustness of the fit, we calculated the transmitted pulse shape for the thin sample, given the same velocities, and compared it to the corresponding data. This method works well, especially at frequencies where the two modes destructively interfere at the output face of the thick sample (Fig. 3). Thus, it was possible to measure the velocities and mean free paths for both modes in pulsed transmission experiments.

B. Multiply scattered ultrasound measurements

In order to take advantage of the excellent monodispersity of the acetate beads, the measurements of scattered ultrasound

were predominately performed on samples made with the 1.2-mm-diameter acetate beads. The beads were randomly packed on top of a thick sheet of polyethelene (whose acoustic impedance is approximately equal to that of water) and held in place by side walls with the top surface open to the water. This apparatus was placed in a large tank of water with a transducer approximately 40 cm underneath the bottom wall to generate a plane wave input pulse. Since acoustic detectors measure the average field across their surface, to measure the scattered ultrasound in the near field without cancellation, one must use a detector whose area is smaller than the speckle size ($\sim\lambda^2$). To measure the transmitted field in a single speckle, we used a miniature hydrophone with a diameter of 0.4 mm suspended about 2 mm above the top surface of the beads. This vertical geometry was used in order to eliminate the effects of a second (top) wall on the scattered sound, thereby simplifying the analysis.

The transmitted field as a function of time was measured in many different speckles by moving the hydrophone to different positions above the sample. Figure 4(a) shows some representative examples of the results at different hydrophone positions. At early times, the signals are dominated by the ballistic pulse (solid line), while at later times, an incoherent scattered component begins to emerge, as indicated by the random phase and amplitude variations of the signal with hydrophone position. In order to isolate the scattered sound, we essentially reversed the process used above for ballistic measurements. We determined the average ballistic pulse [Fig. 4(a)] and subtracted this from the total transmitted sound field, thereby extracting the multiply scattered sound [Fig. 4(b)]. The envelope of the wave field was determined and then squared to calculate the signal that is proportional to the scattered intensity as a function of time for each speckle measured. Averaging together the scattered intensity for each of the speckles gave the ensemble-averaged intensity for the multiply scattered component of the transmitted waves [Fig 4(c)], which was then normalized by the peak intensity in the input pulse.

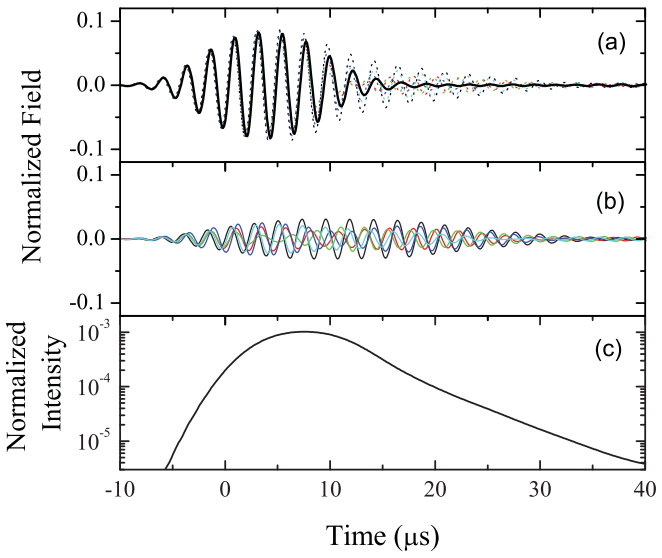

FIG. 4. (Color online) (a) Dotted lines show the total ultrasonic field transmitted through a $L = 9$ mm sample at $2\omega a/v_0 = 2.23$ for several different hydrophone positions (data denoted by different colors); the solid black line shows the average or ballistic waveform. (b) Multiply scattered ultrasound at the same hydrophone positions. (c) Ensemble-averaged scattered intensity. The average bead radius is 0.98 mm.

III. RESULTS AND DISCUSSION

A. Ballistic modes

Using the experimental techniques described in the previous section, we measured the frequency dependence of the ballistic propagation parameters through the two PMMA samples. From the measured phase shift $\Delta\phi$, the wave vector $k = \Delta\phi/L$ was calculated to obtain the dispersion curves plotted in Fig. 5. Excellent agreement between the data for the two sample thicknesses is evident. At low frequencies, there is only one mode, but for $2\omega a/v_0$ above about 2.5, we begin to see evidence of a second propagating mode, as described in the previous section and as shown in Fig. 3. The second mode has been identified as a propagating Stoneley mode,[12,13] resulting from the coupling between the scattering resonances of neighboring spheres. It has a much slower phase velocity and in general a somewhat slower group velocity than the main longitudinal mode. We continue to see both of these modes over the rest of the measured frequency range, up to $2\omega a/v_0 = 5$.

The relative amplitudes of the two modes in our experiments depend not only on the strength of each mode (i.e. the scattering mean free path, l_s, and absorption length, l_a), but also on the relative efficiency of coupling of the incident and outgoing beams into and out of each mode. We find that, over the frequency range of interest, the transmitted amplitudes of the two modes are comparable to each other. The error bars on the relative amplitudes from the two-pulse fitting for the thin sample are too large to extract the coupling coefficients, but

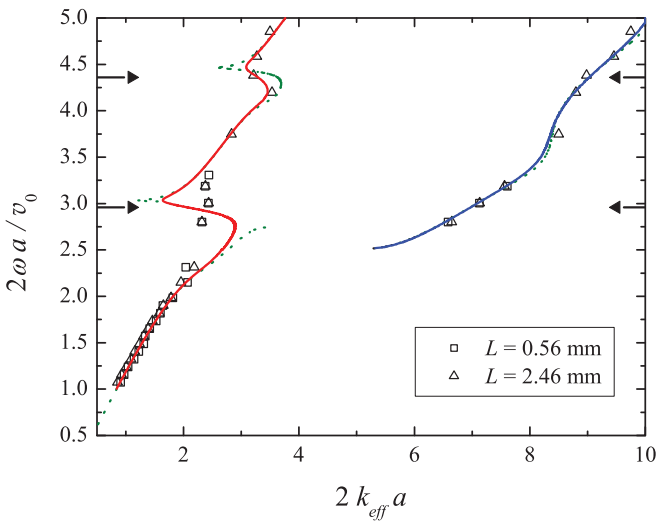

FIG. 5. (Color online) Measured (symbols) and theoretical (lines) dispersion curves. The dashed line has no absorption in the calculation; the solid line includes the effects of absorption with its magnitude being determined from the measured absorption times. The horizontal arrows indicate the resonant frequencies of a single PMMA sphere in water.

we are able to make reliable estimates of the extinction lengths ($1/l_e = 1/l_s + 1/l_a$) of each mode by using the data from the two sample thicknesses. This is possible since the reduction in signal due to coupling losses and boundary reflections is independent of sample thickness, while the contribution due to scattering and absorption depends exponentially on the ratio of sample thickness to extinction length. The experimental results are shown in Fig. 6, where the solid and open symbols represent the extinction lengths for the fast and slow modes respectively. Also, as will be described in the next section, we can obtain a measurement of the absorption length in the sample from the ensemble-averaged scattered intensity. We find that this absorption length is approximately 10 times the extinction length, indicating that the attenuation of the ballistic signal is dominated by scattering. At low frequencies, the extinction length drops precipitously as the frequency increases, but near $2\omega a/v_0 = 2.8$, there appears only to be a quasigap, as the extinction length for the fast mode remains finite at a value that is similar in magnitude to its value at higher frequencies. As was noted previously, in order to ensure that the closing of this quasigap was not only due to the polydispersity of the PMMA spheres, we performed a test using the very monodisperse acetate bead samples and saw the same behavior. Both in the quasigap and at higher frequencies, the extinction lengths for the two modes are quite similar; the extinction lengths are between one and two particle diameters, and they only show a small amount of structure at frequencies in and above the first quasigap.

In order to interpret the measured dispersion curve, we use a spectral function approach, which allows ballistic wave propagation to be described at intermediate frequencies where conventional effective medium approaches breakdown.[12,13,16,17] Although our calculations took the elastic wave nature of ultrasonic waves into account (as described in detail in Ref. 13), it is instructive to illustrate the principles of the technique using the simpler scalar wave case. The scalar wave equation may be written as,

$$\left[\nabla^2 + \frac{\omega^2}{v_{\text{eff}}^2} - \left(\frac{\omega^2}{v_{\text{eff}}^2} - \frac{\omega^2}{v^2(r)}\right)\right]\psi = 0, \tag{1}$$

where ψ denotes the wave amplitude, $v(r)$ is the local phase velocity, and a constant term involving an effective-medium wave speed, v_{eff}, has been added and subtracted. The ensemble-averaged Green's function, $G_e(\omega,\vec{k}_{\text{eff}})$, is given by

$$G_e(\omega,\vec{k}_{\text{eff}}) = \frac{1}{\omega^2/v_{\text{eff}}^2 - k_{\text{eff}}^2 - \Sigma_{v_{\text{eff}}}(\omega,\vec{k}_{\text{eff}})}, \tag{2}$$

where $\Sigma_{v_{\text{eff}}}$ is the self energy calculated relative to the effective medium speed v_{eff}, and $\vec{k}_{\text{eff}}$ is the Fourier transform variable of $\vec{r}$. To the leading order in n, the number density of scatterers,

$$\Sigma_{v_{\text{eff}}} \approx \frac{n f_{v_{\text{eff}}}(0)}{4\pi}, \tag{3}$$

where $f_{v_{\text{eff}}}(0)$ is the forward-scattering amplitude for a single scatterer. Our system may be viewed as a collection of basic units, each made up of solid spheres, coated by a water layer, and embedded in an effective medium, whose phase velocity is identified at each $(\omega,\vec{k}_{\text{eff}})$ point as $v_{\text{eff}} = \omega/k_{\text{eff}}$. The scattering amplitude can then be obtained as the solution to the boundary value problem corresponding to this basic scattering unit.[13,16,17] Thus, from Eq. (3), we obtain the complex values of the self energy $\Sigma_{v_{\text{eff}}} = \Sigma_{\omega/k_{\text{eff}}}(\omega)$ at each point in the $\omega - k_{\text{eff}}$ plane. If we use the condition that $v_{\text{eff}} = \omega/k_{\text{eff}}$, the Green's function is then given by $G_e(\omega,\vec{k}_{\text{eff}}) = -\Sigma^{-1}_{\omega/k_{\text{eff}}}(\omega)$. We can find the modes of excitation of the system by identifying maxima in the spectral function, $-\text{Im}G_e(\omega,\vec{k}_{\text{eff}}) = \text{Im}\Sigma^{-1}_{\omega/k_{\text{eff}}}(\omega)$. A contour plot representing the spectral function calculated in this way is shown in Fig. 1. The maxima in the spectral function are minima in the scattering and thus correspond to the propagating modes of the system. In a propagation experiment, ultrasonic pulses with a particular frequency spectrum are incident on the sample, and the response is measured. Therefore, as alluded to earlier, in order to compare with our experiments, the peaks in the spectral function should be found by holding ω constant and scanning through k_{eff}.

Since, as measured in the scattering experiments, there is considerable absorption in our samples; it was necessary to include the effects of this absorption in the calculation of the spectral function. To do this, we used the measured absorption length in our PMMA samples and assumed that the absorption length depends inversely on frequency throughout the entire frequency range, as suggested by the experimental data. This frequency dependence is also consistent with measurements of dissipation in suspensions of glass beads in water[19] and in bulk PMMA. We then included this absorption in the calculation of the spectral function by allowing the moduli of the constituent materials to be complex, evenly spreading the dissipation over the coating and the solid sphere. By distributing the absorption inside this heterogeneous material in this way, we only approximately model the possible absorption loss mechanisms, which include viscous losses at the interfaces and to a lesser extent bulk absorption losses in the water and plastic. The contour plot in Fig. 7 shows the effect of

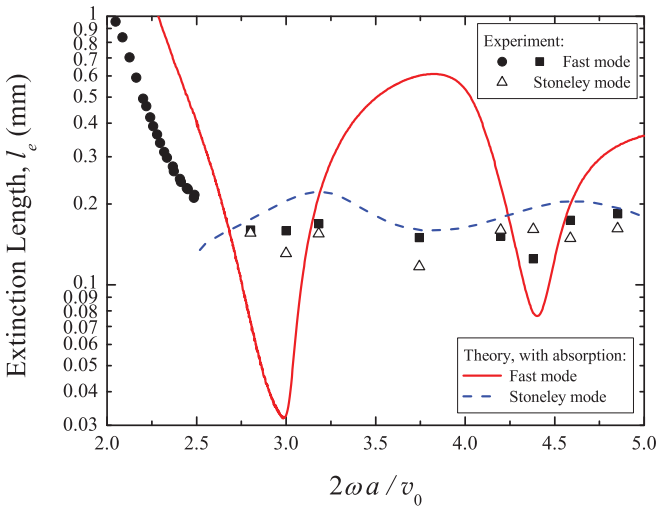

FIG. 6. (Color online) Measured extinction lengths for the fast (solid symbols) and slow modes (open symbols) and the results of the spectral function calculation for both modes with absorption included (solid and dashed lines for the fast and slow modes, respectively).

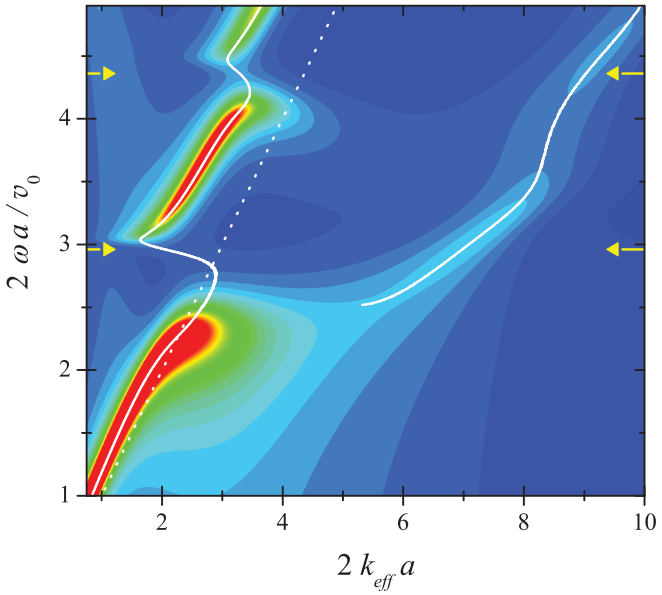

FIG. 7. (Color online) Spectral function for a PMMA sphere/water mixture at a volume fraction of $\phi = 0.55$ with the measured absorption included in the calculation. The solid line is the dispersion curve found when the peaks are located by varying k while holding ω constant. The dotted line gives the dispersion relation for water and the horizontal arrows indicate the resonant frequencies of a single PMMA sphere.

including (measured) absorption in the calculation of the spectral function of PMMA spheres randomly packed in water at a solid volume fraction of $\phi = 0.55$.

The dispersion curve, found by scanning through k_{eff} at constant ω, is also shown in Fig. 7. We contrast Fig. 7 with Fig. 1, in which no absorption was included in the calculation, and a complete gap in the main longitudinal mode (no maxima in the spectral function, indicating no modes) is seen. When absorption is added, Fig. 7 shows that the quasigap closes, and there is a weak longitudinal mode as well as the Stoneley mode, which corresponds to the situation seen in our experiments. It is important to note the sensitivity of ultrasonic measurements to this effect. If one were to hold the wave vector constant and scan through frequency, then this cut through the spectral function shows only a smooth minimum with no peak in the gap. In this case, there would appear to be a complete gap in the fast longitudinal mode, both with and without absorption, as was found in Brillouin scattering experiments.[11] Note also that near $2\omega a/v = 2.5$, there is a range of wave vectors for the slow mode between $2.5 < k_{\text{eff}}a < 5$ in which the spectral function decreases monotonically (no peaks exist) when scanned at constant ω, so the dispersion relation for the slow mode is not resolved. It is also not accessible to ultrasonic transmission measurements for this range of wave vectors.

In Fig. 5, we show the comparison of our experimental data to the dispersion curve calculated with the measured absorption included (solid curves). There is good agreement between theory and experiment at low frequencies, but there are differences for the longitudinal mode once the first quasigap is reached. The experimental data in the quasigap are more smoothed out than the calculation—the theory shows a characteristic zigzag shape with a range of frequencies where the predicted group velocity is negative, while the experiments indicate large but positive group velocity. The difference between theory and experiment near the first quasigap may result from the uniform way in which absorption was included in the calculation, so that effectively it underestimates the effects of absorption on the dispersion curve in this frequency range. This is likely to occur since the absorption and the wave field amplitudes are both spatially inhomogeneous, but the positions where maximum absorption occurs will not necessarily coincide with maxima in the amplitude at these frequencies. Despite this limitation of the model, the calculation shows the necessity of including absorption in the theory as well as the sensitivity of the dispersion relations to absorption at frequencies near band gaps,[20] especially for hybridization gaps associated with scattering resonances. At frequencies above the first gap, including the second smaller gap, the experimental data for both the Stoneley and fast longitudinal modes agree remarkably well with the theoretical calculations. It is worth emphasizing that there are no adjustable parameters in the theory.

We can also use the same theoretical model to calculate the scattering mean free path, yielding the results shown in Fig. 6 by the solid and dashed lines for the fast and slow modes, respectively. Here, the agreement with the data is not as good; the theory has much more structure and is generally larger than the experiment. Once again, if the effective absorption included in the theoretical model were larger, there would be a better correspondence between theory and experiment; however, since a microscopic model for the absorption has not been developed, it is not really meaningful to attempt to achieve a better description of the data by imposing an average absorption that differs significantly from that measured in our scattered ultrasound measurements.

B. Multiply scattered ultrasound

Measurements were taken on two acetate bead samples with thicknesses of 9.0 and 13.0 mm and at frequencies spanning a range from below to above the lowest quasigap in the dispersion curve. Figure 8 shows the ensemble-averaged scattered intensities transmitted through these samples at several frequencies. The magnitude of the scattered signals is surprisingly small, especially when compared to the ballistic signals, which are larger than the scattered signals (see Fig. 4), in spite of L/l_s being of the order of 10 for the thicker sample. In fact, at frequencies in the first quasigap, we were unable for the thicker sample to make reliable measurements of the scattered component above the background level. One possible explanation for this behavior is the very strong absorption in the samples.

Diffusion theory has been found to provide an accurate description of multiply scattered ultrasonic wave transport through strongly scattering materials for a wide range of scattering strengths and sample thicknesses.[18] It is therefore used here to interpret our results. The diffusion approximation neglects all phase information and models the transport of scattered ultrasound energy as a random walk through the sample with a path step given by the transport mean free path l^*, a velocity given by the energy velocity v_E, dissipation

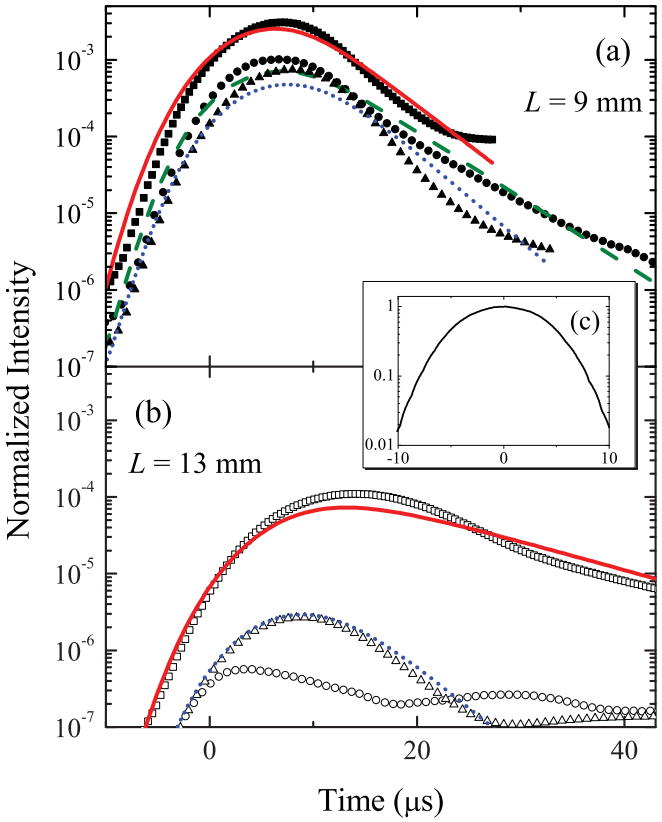

FIG. 8. (Color online) Measured ensemble-averaged scattered intensity for (a) the $L = 9$-mm- and (b) $L = 13$-mm-thick samples at several frequencies. The squares are data at $2\omega a/v_0 = 1.82$, and the solid line is a fit of diffusion theory to these data. Circles are at $2\omega a/v_0 = 2.23$ with a dashed fit, and triangles are at $2\omega a/v_0 = 2.84$ with a dotted fit. The inset (c) shows the corresponding input pulse intensity.

described by an absorption time τ_a, and a diffusion coefficient given by

$$D = \tfrac{1}{3} v_E l^*. \tag{4}$$

When there are two modes that are mixed by scattering, the diffusion approximation can still be used, but the average transport is now described in terms of an average effective diffusion coefficient, energy velocity, and transport mean free path. Assuming equipartition of the energy between the modes of the system and the simplest approximation for the energy density at a given frequency ($U \propto 1/v_{\mathrm{ph}}^3$), the effective diffusion coefficient (given by the energy density weighted average) can be written, in analogy to the equipartition of elastic waves[21–23] as:

$$D_{\mathrm{eff}} = \frac{\frac{D_L}{v_{\mathrm{ph,L}}^3} + \frac{D_S}{v_{\mathrm{ph,S}}^3}}{\frac{1}{v_{\mathrm{ph,L}}^3} + \frac{1}{v_{\mathrm{ph,S}}^3}}, \tag{5}$$

where D_L and D_S are the partial diffusion coefficients for the fast longitudinal and Stoneley modes, respectively.

In particulate suspensions, the energy velocity has been found to be nearly equal to the group velocity and the transport mean free path to be close to the scattering mean free path.[24] However, the first relationship will not hold true for the longitudinal mode in the quasigap when its group velocity is very large or perhaps even negative. The group velocity of each of the two modes can be measured from the slope of their respective dispersion curves, and as described previously, the scattering mean free path of each mode has been measured. Fits of diffusion theory to the ensemble-averaged scattered intensity, using the appropriate boundary conditions,[18] enable the diffusion coefficient D and the absorption time τ_a to be measured. Thus, at frequencies above and below the quasigap, the measured values of D can be compared with estimates based on the ballistic parameters using Eqs. (4) and (5), with $v_E \approx v_g$ and $l^* \approx l_s$.

The fits of diffusion theory to the average time-dependent transmitted intensity are shown by the lines in Fig. 8. In panel (a), the data and fits for the 9-mm-thick sample are shown, while panel (c) shows a representative input pulse. By comparing the width of the input pulse to the thin sample data, it is clear that the multiple scattering does not extend over very long propagation times, as most of the width of the diffusive signal is similar to the finite width of the input pulse. Nonetheless, with the width of the input pulse correctly taken into account, the fits of diffusion model give a reasonably good description of the data for both the thin and thick samples [Figs. 8(a) and 8(b)]. However, the overall magnitude of the transmitted intensity is much less than that predicted by diffusion theory, an effect which was accounted for in the fits

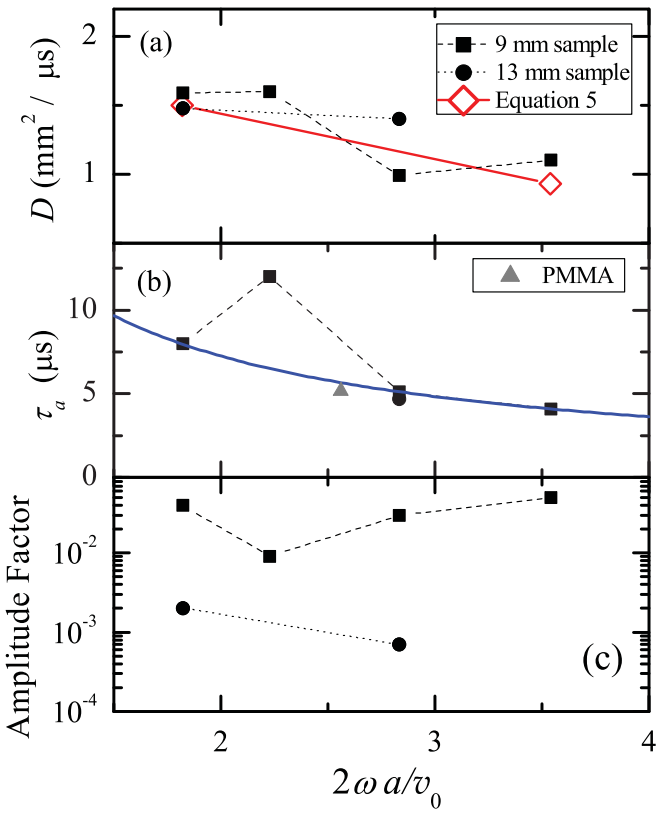

FIG. 9. (Color online) Measured diffusion parameters as a function of frequency: (a) Diffusion coefficient (solid symbols) with the values calculated from Eq. (5) (open diamonds). (b) Absorption time with the solid curve showing a fit to a ω^{-1} behavior. (c) Amplitude factor.

by an amplitude factor, $A < 1$. The parameters obtained from the fits of diffusion theory to the ensemble averaged scattered intensity data are shown in Fig. 9 for several frequencies. Note that the long time tail is approximately exponential and that within the diffusion model the decay constant is

$$\frac{1}{\tau} = \frac{\pi^2 D}{L_{\text{eff}}^2} + \frac{1}{\tau_a}, \tag{6}$$

where $L_{\text{eff}} > L$ is the effective thickness of the sample, which is larger than L by the distance over which the diffuse intensity extrapolates to zero outside the sample.[25] For the values of D and τ_a shown in Fig. 9, this equation indicates that the long time decay is dominated by absorption. Thus, the diffusion fit should give a reliable estimate of the absorption time in the sample, independent of the surprisingly small amplitude factor and insensitive to uncertainties in D.

Figure 9(a) also compares the measured values of D from the multiply scattered intensity profiles with values of the diffusion coefficients estimated from Eq. (5), using estimates of the transport mean free path and the energy velocity from the ballistic data. Remarkably good agreement is found both below and above the quasigap. As well, consistent values of the diffusion coefficients and absorption times are obtained from the fits of the diffusion approximation to the data for the two sample thicknesses. Thus, even though the quality of the data for the time-of-flight intensity profiles is not as good as in some other systems[18] because the multiply scattered signals are so small, reliable values of D and τ_a were obtained from the fits. The results for the absorption time extend over a wide enough frequency range for the frequency dependence to be investigated: as shown by the solid curve in Fig. 9(b), we can see that the absorption time is inversely proportional to the frequency (with the exception of one anomalous point at $2\omega a/v_0 \approx 2.2$, near the bottom of the quasigap). Also shown on the same graph is the absorption time measured at one frequency for a PMMA sample, which is consistent with the data for the acetate beads. These results were used to determine the values of the absorption incorporated in the effective medium model for the ballistic data discussed in Sec. III A.

IV. CONCLUSIONS

Ultrasonic pulse propagation experiments in suspensions of plastic spherical scatterers provide an excellent way of studying the effects of scattering resonances on wave transport in random media. By separating the coherent ballistic component from the multiply scattered wave field, both the dispersion relations and the diffusive propagation of ultrasound have been studied in this system. The dispersion relation is marked by a series of hybridization gaps due to the coupling between the propagating modes of surrounding fluid and the scattering resonances, which involve interfacial modes of the spheres. Our ultrasonic experiments and effective medium theory show that the hybridization gaps are partially closed when absorption is present, an effect that is not evident in previous Brillouin scattering experiments on this system. This effect is demonstrated not only by the shape of the experimental dispersion relation but also by the predictions of our effective medium model, which enables the dispersion relations to be compared both without and with absorption. This theory is based on a spectral function approach and gives a description of the dispersion relations in this system that is in good overall agreement with the experimental data. The coupling between the scattering resonances on adjacent spheres leads to the formation of an additional longitudinal branch in the dispersion relation, which is also seen in our experiments. This combination of pulsed ultrasonic experiments and theory has enabled an in-depth study of hybridization gaps and how they are affected by absorption, a topic of current interest in the context of phononic crystals, where hybridization provides an alternate mechanism to Bragg scattering for creating band gaps in ordered systems.

Despite the very strong scattering in this system at intermediate frequencies, there is a surprisingly small amount of scattered sound transmitted through the samples. Absorption likely accounts for most but perhaps not all of this. Nonetheless, it was possible to measure the transport of multiply scattered ultrasound through the samples for a limited range of propagation times. By fitting the data with predictions of the diffusion approximation, reliable values of both the diffusion coefficient and absorption time were measured. The diffusion coefficient is consistent with simple estimates based on the ballistic parameters, giving a rather complete picture of wave transport in this system. Since the scattering length is an order of magnitude smaller than the absorption length, the exponential decay with distance of the coherent ballistic signal is dominated by scattering, making it impossible to determine the absorption directly from ballistic pulse propagation experiments. Hence, the direct measurement of the absorption that was made from the decay of the multiply scattered wave intensity with time is especially useful. These measurements show that the absorption increases linearly with frequency, a result that is consistent with other experiments on random systems.

ACKNOWLEDGMENT

Financial support from NSERC of Canada is gratefully acknowledged.

*Present address: Attodyne Inc., 60 George St., Toronto ON M5S 1A7.

†Corresponding author: jhpage@cc.umanitoba.ca

[1] P. Sheng, *Introduction to Wave Scattering, Localization, and Mesoscopic Phenomena* (Springer, Heidelberg, 2006).

[2] J. D. Joannopoulos, R. D. Meade, and J. N. Winn, *Photonic Crystals: Molding the Flow of Light* (Princeton University Press, Princeton, 1995).

[3] I. E. Psarobas, A. Modinos, R. Sainidou, and N. Stefanou, Phys. Rev. B **65**, 064307 (2002).

[4]T. Still, W. Cheng, M. Retsch, R. Sainidou, J. Wang, U. Jonas, N. Stefanou, and G. Fytas, Phys. Rev. Lett. **100**, 194301 (2008).
[5]V. Leroy, A. Strybulevych, M. G. Scanlon, and J. H. Page, Eur. Phys. J. E **29**, 123 (2009).
[6]V. Leroy, A. Bretagne, M. Fink, H. Williams, and P. Tabeling, Appl. Phys. Lett. **95**, 171904 (2009).
[7]*Physics of Negative Refraction and Negative Index Materials*, edited by C. M. Krowne and Y. Zong (Springer, Berlin, 2007).
[8]J. B. Pendry, Phys. Rev. Lett. **85**, 3966 (2000).
[9]Z. Y. Liu, X. X. Zhang, Y. W. Mao, Y. Y. Zhu, Z. Y. Yang, C. T. Chan, and P. Sheng, Science **289**, 1734 (2000).
[10]Z. Yang, J. Mei, M. Yang, N. H. Chan, and P. Sheng, Phys. Rev. Lett. **101**, 204301 (2008).
[11]J. Liu, L. Ye, D. A. Weitz, and P. Sheng, Phys. Rev. Lett. **65**, 2602 (1990).
[12]X. D. Jing, P. Sheng, and M. Y. Zhou, Phys. Rev. Lett. **66**, 1240 (1991).
[13]X. D. Jing, P. Sheng, and M. Y. Zhou, Phys. Rev. A **46**, 6513 (1992).
[14]R. S. Penciu, H. Kriegs, G. Petekidis, G. Fytas, and E. N. Economou, J. Chem. Phys. **118**, 5224 (2003).
[15]G. Tommaseo, G. Petekidis, W. Steffen, G. Fytas, A. B. Schofield, and N. Stefanou, J. Chem. Phys. **126**, 014707 (2007).
[16]J. H. Page, P. Sheng, H. P. Schriemer, I. Jones, X. D. Jing, and D. A. Weitz, Science **271**, 634 (1996).
[17]M. L. Cowan, K. Beaty, J. H. Page, Z. Y. Liu, and P. Sheng, Phys. Rev. E **58**, 6626 (1998).
[18]J. H. Page, H. P. Schriemer, A. E. Bailey, and D. A. Weitz, Phys. Rev. E **52**, 3106 (1995).
[19]J. H. Page, H. P. Schriemer, I. P. Jones, P. Sheng, and D. A. Weitz, Physica A **241**, 64 (1997).
[20]S. X. Yang, J. H. Page, Z. Y. Liu, M. L. Cowan, C. T. Chan, and P. Sheng, Phys. Rev. Lett. **88**, 104301 (2002).
[21]R. L. Weaver, J. Mech. Phys. Solids **38**, 55 (1990).
[22]L. Ryzhik, G. Papanicolaou, and J. B. Keller, Wave Motion **24**, 327 (1996).
[23]N. P. Tregoures and B. A. van Tiggelen, Waves in Random Media **12**, 21 (2002).
[24]H. P. Schriemer, M. L. Cowan, J. H. Page, P. Sheng, Z. Y. Liu, and D. A. Weitz, Phys. Rev. Lett. **79**, 3166 (1997).
[25]J. X. Zhu, D. J. Pine, and D. A. Weitz, Phys. Rev. A **44**, 3948 (1991).